JACS
JOURNAL OF THE AMERICAN CHEMICAL SOCIETY

ARTICLE

pubs.acs.org/JACS

High Performance Na-doped PbTe–PbS Thermoelectric Materials: Electronic Density of States Modification and Shape-Controlled Nanostructures

Steven N. Girard,[†] Jiaqing He,[†,‡] Xiaoyuan Zhou,[§] Daniel Shoemaker,[∥] Christopher M. Jaworski,[⊥] Ctirad Uher,[§] Vinayak P. Dravid,[‡] Joseph P. Heremans,[⊥] and Mercouri G. Kanatzidis*[,†,∥]

[†]Department of Chemistry, and [‡]Department of Materials Science and Engineering, Northwestern University, Evanston, Illinois 60208, United States

[§]Department of Physics, University of Michigan, Ann Arbor, Michigan 48109, United States

[∥]Materials Science Division, Argonne National Laboratory, Argonne, Illinois 60439, United States

[⊥]Department of Physics, Ohio State University, Columbus, Ohio 43210, United States

Supporting Information

ABSTRACT: Thermoelectric heat-to-power generation is an attractive option for robust and environmentally friendly renewable energy production. Historically, the performance of thermoelectric materials has been limited by low efficiencies, related to the thermoelectric figure-of-merit ZT. Nanostructuring thermoelectric materials have shown to enhance ZT primarily via increasing phonon scattering, beneficially reducing lattice thermal conductivity. Conversely, density-of-states (DOS) engineering has also enhanced electronic transport properties. However, successfully joining the two approaches has proved elusive. Herein, we report a thermoelectric materials system whereby we can control both nanostructure formations to effectively reduce thermal conductivity, while concurrently modifying the electronic structure to significantly enhance thermoelectric power factor. We report that the thermoelectric system PbTe–PbS 12% doped with 2% Na produces shape-controlled cubic PbS nanostructures, which help reduce lattice thermal conductivity, while altering the solubility of PbS within the PbTe matrix beneficially modifies the DOS that allow for enhancements in thermoelectric power factor. These concomitant and synergistic effects result in a maximum ZT for 2% Na-doped PbTe–PbS 12% of 1.8 at 800 K.

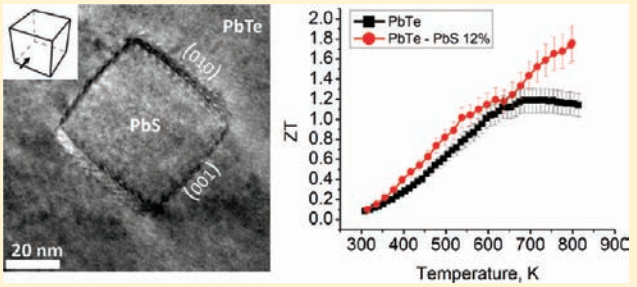

INTRODUCTION

Within the past decade, significant increases in the efficiency of thermoelectric materials have attracted widespread research interest in potential applications for waste heat-to-electricity conversion. The efficiency of thermoelectrics is related to the thermoelectric figure-of-merit ZT, which is defined as $ZT = (S^2\sigma T/\kappa)$, where T is the operating temperature, S is the Seebeck coefficient or thermopower, σ is electrical conductivity, and κ is thermal conductivity. Recently, the nanostructuring of thermoelectric materials has provided impressive increases in ZT, primarily as a result of reduced lattice thermal conductivity. This has been demonstrated both for nanostructured bulk thermoelectric materials[1−3] as well as for nanoparticle, nanowire, and nanoscale superlattice materials.[4−8] A wealth of research in this area has demonstrated that the effective scattering of phonons by nanostructures can reduce lattice thermal conductivity while not deleteriously affecting electronic transport.[9−16] However, many of these materials systems are reaching their limit of lattice thermal conductivity reduction, and to further increase ZT researchers must now consider methods to concurrently increase the power factor ($S^2\sigma$).

When considering the electronic transport properties of degenerate semiconducting thermoelectric materials, one must find the optimal carrier concentration at which electrical conductivity and thermopower have maximal power factor. In practice, this can be challenging because electrical conductivity and thermopower are inversely proportional with respect to carrier concentration, assuming parabolic energy dependence and no change in carrier effective mass. Because of this, there are inherent limitations to the magnitude of the power factor that can be obtained for conventional thermoelectric materials. To circumvent this issue, researchers have begun manipulating the electronic structure of thermoelectrics through purposeful alteration of the electronic density of states (DOS). Through doping with Tl, Heremans et al. reported a doubling in ZT of thermoelectric *p*-type PbTe through a beneficial distortion of the DOS

Received: July 9, 2011
Published: September 08, 2011

ACS Publications © 2011 American Chemical Society

near the Fermi level, which increases the effective mass of the holes. This results in significantly enhanced values of thermopower without a marked reduction in electrical conductivity.[17] The higher power factor in this system allows for a higher ZT virtually without any reduction in lattice thermal conductivity; unlike the majority of the impetus in the field, this work presented a wholly non-nanostructured means of achieving high ZT. Since then, significant efforts have been invested toward developing thermoelectric materials wherein the electronic structure may be advantageously modified to boost ZT.[18−22]

Recently, our research group has shown that in heavily doped *p*-type PbTe, interplay between the light and heavy valence bands in PbTe at high temperature can result in significant increases to power factor.[20] Failure of a single-band model for *p*-type PbTe prompted Allgaier and coworkers to devise a model evidencing the presence of two valence bands in PbTe.[23,24] The nonparabolic principal band is characterized by a narrow dispersion within the DOS and light effective mass $0.2-0.36m_0$, while the secondary band lies approximately 0.05−0.1 eV below that of the principal, is highly parabolic, widely dispersed within the DOS, and exhibits a much heavier effective mass $1.2-2m_0$.[25] For this reason, they are referred to as the light and heavy valence bands, respectively. Because of differences in dispersion and effective mass, the hole transport within the two bands is significantly different, and promoting carriers to the heavy hole band may significantly increase thermopower. Through increasing the hole concentration $>10^{19}$ cm^{-3} in Na/K codoped PbTe, Androulakis et al.[20] showed that effective pinning of the Fermi level allows significant promotion of carriers from the light- to heavy-hole bands at elevated temperatures. Kudman[26] was first to show, and more recently confirmed by Pei,[22] the enhancement in thermoelectric figure of merit in PbTe−PbSe alloys doped with Na. Substitution of Te by Se effectively tunes the location of the valence bands of PbTe, which at high doping can maximize promotion of carriers into the heavy hole band to enhance power factor. The thermoelectric properties appear to be heavily dependent on proper PbSe and Na alloying to allow a high ZT. Without inducing a resonance state within the DOS, these works showed advantageous band structure engineering to achieve high power factors from bulk non-nanostructured material. What is lacking in the literature, at this point, is any report of the successful combination of a nanostructured thermoelectric material with a concomitantly enhanced electronic structure.

Herein, we report a thermoelectric system exhibiting both desirable electronic structure modification of the DOS to increase power factor in addition to nanostructuring to reduce lattice thermal conductivity as has been demonstrated previously,[27,28] and we show that PbTe−PbS produce naturally formed nanostructures that we attribute to the low lattice thermal conductivities of the materials. Additionally, we report the first successful shape control of the PbS nanostructures through changing the concentration of Na and PbS, producing cuboctahedral shapes of PbS nanocrystals that are coherently embedded throughout the PbTe matrix. Structural characterization and properties measurements show that small amounts of PbS alloying within the PbTe matrix appear to modify the location of the heavy and light valence bands of PbTe. Through doping with Na, we show enhancement in the electronic transport through promotion of carriers between the heavy and light bands, producing a high thermoelectric power factor despite reductions in electrical conductivity in comparably doped nominal Na-doped PbTe. As a result of these effects, we achieve a maximum ZT of 1.8 at 800 K for the 2% Na-doped PbTe−PbS 12% composition.

EXPERIMENTAL SECTION

Synthesis. Stock Na-doped $Pb_{1-x}Na_xTe$ and $Pb_{1-x}Na_xS$ (x = 0.005, 0.01, 0.015, 0.02) were prepared from high-quality starting materials (Te 99.999% 5N Plus, Pb 99.99% American Elements, S 99.99% 5N Plus, and Na 99.9% Sigma-Aldrich) from the reaction between each constituent in carbon-coated sealed fused silica tubes under high vacuum ($\sim10^{-4}$ Torr) at temperatures above the material melting point. Purity of starting materials was verified by powder X-ray diffraction. Corresponding samples of $Pb_{1-x}Na_xS_yTe_{1-y}$ (two sets: one where x = 0.02 and y = 0.04, 0.08, 0.12, 0.16, and 0.30, and the other where y = 0.12 and x = 0.02, 0.015, 0.01, and 0.005) were then synthesized in evacuated carbon-coated fused silica tubes using stock the Na-doped PbTe, PbS. The samples were heated to 1100 °C, held at the liquid state for several hours, and rapidly cooled in-furnace to room temperature. Homogeneity of samples from top to the bottom of the ingot was verified both by powder X-ray diffraction and by Scanning Electron Microscope and Energy Dispersive X-ray Spectroscopy (SEM/EDS) analysis. The resulting material is easily cut and polished, then characterized and analyzed for thermoelectric properties.

Powder X-ray Diffraction. Finely ground samples were placed in a CPS-120 Inel X-ray powder diffractometer using Ni-filtered Cu K_α radiation (λ = 1.54056 Å) in reflection geometry, equipped with a position sensitive detector and operating at 40 kV and 20 mA. Le Bail refinements were performed using the GSAS program.

Electrical Conductivity and Thermopower/Seebeck Coefficient Measurements. Electrical transport measurements were performed on two instrumental systems, at Northwestern University (NU) and University of Michigan (UM). All samples included in this study were measured on the NU system, and high-temperature (>800 K) measurements were verified for accuracy on both systems as described in the text.

At NU, electrical conductivity and thermopower/Seebeck coefficient were measured on polished parallelepipeds approximately 2 × 2 × 10 mm in an ULVAC ZEM-3 electrical conductivity and Seebeck coefficient system. Samples were sandwiched between two Ni electrodes with two probe thermocouples providing forced contacts on one side. Sample surfaces were protected from the electrodes and thermocouples using graphite foil. Electrical conductivity measurements were accomplished using a standard four-probe setup. A resistive heater on the lower electrode provided nominal temperature differentials of 10, 20, and 30 °C to determine the Seebeck coefficient. The sample chamber was evacuated and backfilled with approximately 0.1 atm He, and heated from room temperature to 950 K using an IR furnace.

At UM, high temperature Seebeck coefficient and electrical resistivity from 300 to 850 K were measured using a home-built apparatus consisting of a hinged tubular oven located under a glass bell jar that was evacuated and backfilled with argon. A sample was attached to a tungsten heat sink located in the center of the oven with either Ag paint or graphite paste, and a small wire-wound heater was affixed at the other end of the sample. The temperature difference at two points along the length of the sample was measured with a pair of very fine R-type Pt versus Pt−Rh thermocouples fastened to the sample with Ag paint. Platinum legs of the thermocouples served as voltage probes. The fine Pt/Pt−Rh wires were in turn clamped to heavy Pt/Pt−Rh wires that were brought out of the oven and attached to copper feed-through pins on a copper block serving as a reference junction. By sweeping a temperature gradient while measuring the corresponding Seebeck voltage, the Seebeck coefficient was determined from the slope of the linear fit and corrected for the thermopower of Pt legs.

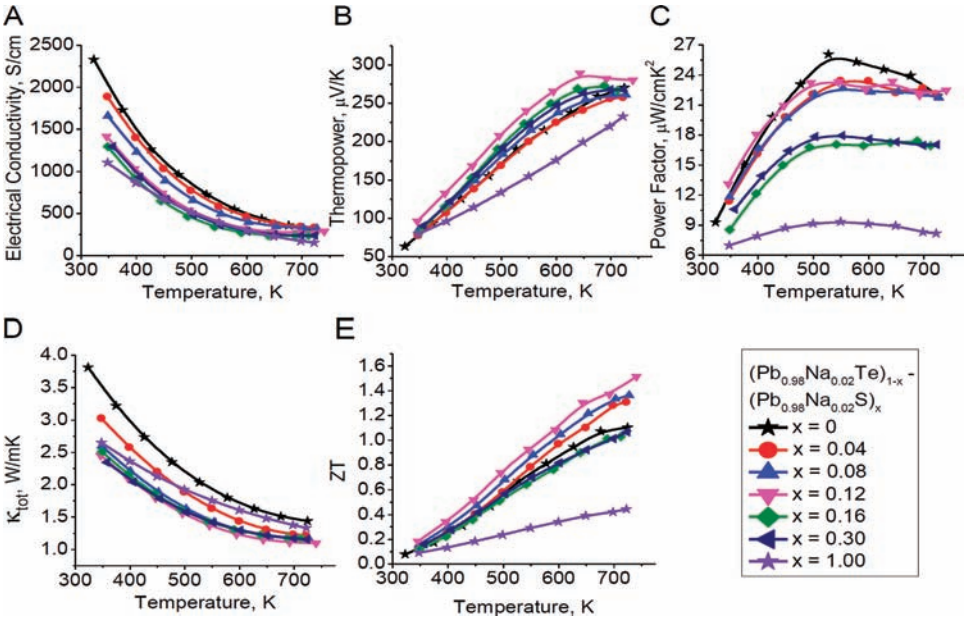

Figure 1. (A) Electrical conductivity, (B) thermopower, (C) power factor, (D) total thermal conductivity, and (E) ZT of 2% Na-doped PbTe, PbS, and PbTe−PbS thermoelectric materials. For clarity, the PbTe and PbS benchmark materials have been labeled with star symbols. Despite a reduction in electrical conductivity, PbTe−PbS materials at or below 12% concentrations still possess high power factors close to that of pure Na-doped PbTe.

Electrical resistivity was measured by the four-probe technique using short current pulses of alternate polarities to minimize a contribution from the Peltier effect.

Hall Measurements. High temperature Hall effect measurements were carried out by an in-house high temperature/high magnetic field Hall apparatus. It consisted of a nine Tesla air-bore superconducting magnet with a water-cooled oven inside the bore of the magnet, and a Linear Research AC bridge with 16 Hz excitation. Four-wire AC Hall measurements were performed on parallelepiped samples with a typical size of 1.5 × 3 × 10 mm to temperatures of 850 K under argon atmosphere.

Thermal Conductivity. Thermal diffusivity and specific heat of samples were measured on a Netzsch LFA 457, using pyroceram 9606 as a reference. Coins measuring approximately 8 mm in diameter by 2 mm in thickness were heated from room temperature to 950 K. Density was calculated from the sample dimensions and mass; corresponding densities were ≥95% theoretical density. Assuming the law of mixtures, specific heat of the samples was estimated using established literature values for corresponding ideal mixtures of PbTe and PbS.[10] Total thermal conductivity was calculated using the equation $\kappa_{tot} = \alpha C_p d$, where κ_{tot} is total thermal conductivity, α is measured thermal diffusivity, C_p is specific heat, and d is density. The electronic contribution to total thermal conductivity κ_{elec} was calculated using the Wiedemann−Franz law, $\kappa_{elec} = \sigma TL$ (where σ = electrical conductivity, T = temperature, and L is either 2.45×10^{-8} W Ω K^{-2} or a calculated value as described in the text). The lattice component κ_{lat} is then calculated using the relation $\kappa_{lat} = \kappa_{tot} - \kappa_{elec}$.

Transmission Electron Microscopy (TEM). TEM samples were prepared by conventional polishing and dimpling in a water-free environment, followed by ion milling at liquid nitrogen temperature. Select specimens were also prepared by FIB/SEM to obtain thin sections for TEM analysis, as described before.[29] TEM investigations were carried out in a JEOL 2100F transmission electron microscope operating at 200 kV accelerating voltage.

RESULTS

Thermoelectric Properties of 2% Na-Doped PbTe, PbS, and PbTe−PbS. Initially, 2% Na-doped PbTe−PbS thermoelectric materials were synthesized. Previous work as well as work in our laboratory has shown that a substitution of 2% Na for Pb provides sufficient donor impurity sites to allow for high power factors.[19,21,30]

The thermoelectric properties and figure of merit of 2% Na-doped PbTe−PbS materials are shown in Figure 1. The reduction in electrical conductivity and concurrent increase in thermopower with increasing PbS concentration are a function of both reduced hole mobilities as well as a slight variation in carrier concentration, Figure 1A and B. However, Na-doped PbS has a significantly lower thermopower when compared to the PbTe-based counterparts. This is because the heavy hole band lies much lower in energy relative to the light hole valence band and does not contribute to the charge transport properties.[31] The power factor in the Na-doped PbTe−PbS materials is high, producing values above 20 μW/cm·K^2 for compositions at and below PbTe−PbS 12%, Figure 1C.

The total thermal conductivities of the PbTe−PbS materials are reduced over the entire temperature range in comparison to that of PbTe, Figure 1D, with values for PbTe−PbS at 750 K approaching 1.0 W/mK as compared to 1.5 W/mK for PbTe. Consequently, the PbTe−PbS materials with concentrations at and below PbTe−PbS 12% show marked improvements in ZT over pure Na-doped PbTe, Figure 1E, with the highest ZT observed for the PbTe−PbS 12% composition.

Lattice thermal conductivities may be estimated using the Wiedemann−Franz law, whereby the electronic contribution to thermal conductivity (κ_{elec}) is calculated using temperature, measured electrical conductivity, and the Sommerfeld Lorenz number (L_0) of 2.45×10^{-8} Ω W K^{-2} according to $\kappa_{elec} = L\sigma T$.[32,33] The lattice thermal conductivity (κ_{lat}) may then be calculated from the total thermal conductivity (κ_{tot}) using the relation $\kappa_{lat} = \kappa_{tot} - \kappa_{elec}$. Although the Lorenz number is assumed to be constant, previous work suggests that for PbTe, the Lorenz number can in fact be reduced to almost one-half the Sommerfeld value at elevated temperatures.[34,35] A more accurate estimation of the Lorenz number as a function of temperature may be accomplished through fitting the reduced chemical

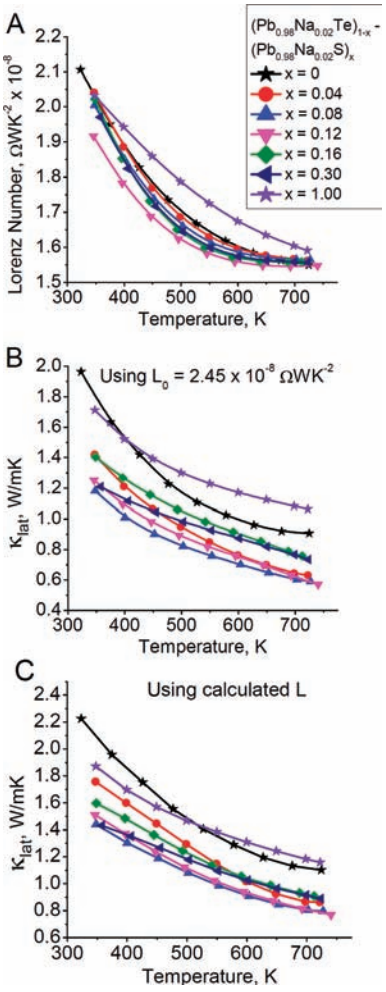

Figure 2. (A) Calculated Lorenz number, (B) lattice thermal conductivity using L_0, and (C) lattice thermal conductivity using calculated L from (A) for 2% Na-doped PbTe, PbS, and PbTe−PbS thermoelectric materials. Significant reductions in lattice thermal conductivity are obtained for PbTe−PbS materials relative to their parent PbTe or PbS composition as a result of the naturally formed nanostructures. The lowest values of lattice thermal conductivity are obtained for the PbTe−PbS 8% and 12% compositions between ~0.5 and 0.75 W/mK at 750 K.

potential η obtained from thermopower data:[33]

$$S = \frac{k}{e}\left(\frac{2F_1(\eta)}{F_0(\eta)} - \eta\right) \quad (1)$$

The η values that fit the temperature-dependent thermopower S can be used to calculate L through:[36]

$$L = \left(\frac{k}{e}\right)^2 \frac{3F_0(\eta)F_2(\eta) - 4F_1(\eta)^2}{F_0(\eta)^2} \quad (2)$$

In this calculation, it is assumed that a single parabolic band is dominated entirely by acoustic phonon scattering and the thermopower may be properly fitted assuming a known effective mass m^*. However, because two bands can contribute to p-type conduction in PbTe especially at higher temperatures, this model may be insufficient at properly describing the Lorenz number and hence the calculation of lattice thermal conductivity. Nevertheless, we show the calculated values of the Lorenz number using the above assumption, and lattice thermal conductivities obtained using both the Sommerfeld L_0 as well as the calculated values, Figure 2A−C. In comparison with 2% Na-doped PbTe and PbS as reference materials, it is clear that the lattice thermal conductivity of Na-doped PbTe−PbS materials is strongly reduced, producing values at high temperature that are 60−70% that of PbTe, Figure 2B and C. The lowest lattice thermal conductivities between 0.55 and 0.75 W/mK are observed for the PbTe−PbS 8% and 12% compositions, in close agreement with previous work showing compositions in this range to have the lowest lattice thermal conductivity.[27,28] It is also important to note that in our calculations of specific heat used in the total thermal conductivity, we assume complete alloying of the PbTe and PbS phases. As we discuss later, the alloying of the phases is not ideal; we are therefore likely overestimating the specific heat contribution to thermal conductivity. Using these data, the combination of high power factor and reduced thermal conductivity produces the largest ZT for the PbTe−PbS 12% composition.

Thermoelectric Properties of Variably Na-Doped PbTe−PbS 12%. In addition to a significant reduction in the lattice thermal conductivity, the 2% Na-doped PbTe−PbS 4%, 8%, and 12% compositions possess high power factors as shown in Figure 1C. To better understand this phenomenon, we selected the highest ZT material of PbTe−PbS 12%. We then varied the carrier concentration by substituting 0.5%, 1%, 1.5%, and 2% Na for Pb and measured to temperatures up to 850 K. The resulting thermoelectric properties are shown in Figure 3. Surprisingly, we observe dissimilar electronic transport as a function of Na doping, particularly in the temperature range >650 K. For 2% and 1.5% Na doping concentrations, electrical conductivity increases between 650 and 850 K, in contrast with the 1% and 0.5% Na-doped samples as well as the 2% Na-doped PbTe standard. Simultaneously, the thermopower data for the 2%, 1.5%, and 1% Na-doped samples show two different regions of temperature dependence, 300−650 and 650−850 K, Figure 3B, wherein the lower temperature range obeys the linearity expected within a single-band model, while in the higher temperature range the thermopower abruptly plateaus, leveling off in a manner uncharacteristic of bipolar diffusion, as shown for the 0.5% Na-doped sample.

The electrical conductivity and thermopower of PbTe−PbS 12% doped with 1−2% Na are highly uncharacteristic of pure PbTe and indicate a significant deviation from typical charge transport assuming single parabolic bands. These results are observed only when we incorporate PbS with PbTe and at high enough Na doping concentrations, indicating that the incorporation of PbS in PbTe at high carrier concentrations is the key. Because of this, the 2% and 1.5% Na-doped PbTe−PbS 12% materials effectively reach a plateau in the power factor from 450 to 850 K, Figure 3C. The effect is most notable for 2% Na-doped PbTe−PbS 12%, where the values of power factor remain above 20 μW/cm·K^2 over the said temperature range, rivaling that of pure 2% Na-doped PbTe. Similar values of the total thermal conductivity for the 2%, 1.5%, and 1% Na-doped PbTe−PbS 12% samples produce differences in ZT largely based on the values of power factor, Figure 3D and E. We see significant enhancements in ZT over that of PbTe for the 2% and 1.5% Na-doped concentrations.

We calculated lattice thermal conductivity in the same way as described previously, Figure 4. Surprisingly, we find that the Na doping concentration also plays an important role in the lattice thermal conductivity reduction, producing the lowest value

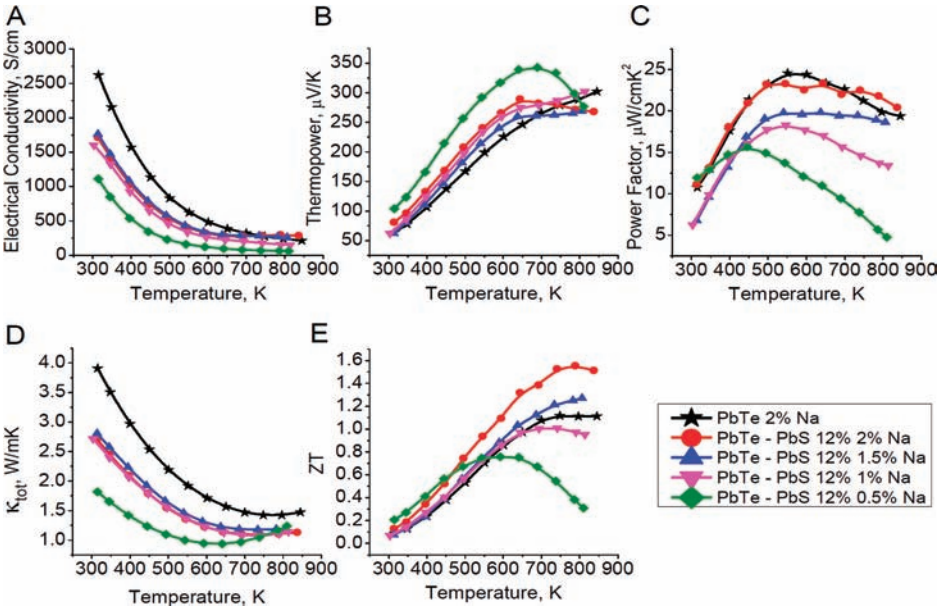

Figure 3. (A) Electrical conductivity, (B) thermopower, (C) power factor, (D) total thermal conductivity, and (E) ZT of 2%, 1.5%, 1%, and 0.5% Na-doped PbTe−PbS 12% thermoelectric materials. Optimal power factors and ZT are obtained for the 2% Na-doped composition. At Na doping of less than 1%, the significant deviation in the electrical transport trends indicates fewer holes are propagating into the heavy hole valence band of PbTe because of the lower carrier concentration.

between 0.5 and 0.75 W/mK at 800 K for the 2% Na-doped sample, Figure 4B and C. Here, we show unequivocally that the 2% Na-doped PbTe−PbS 12% is optimal for enhancing the power factor as in Figure 3C, and in reducing the lattice thermal conductivity.

To further elucidate on the observed effects, we have conducted high-temperature Hall effect studies of the variably doped PbTe−PbS 12% samples. The hole concentration n was calculated from the Hall coefficient R_H using the equation $n = 1/eR_H$, again assuming single degenerate parabolic dispersion. The hole mobility μ was then calculated using $\mu = \sigma/ne$. The results are shown in Figure 5A and B. There exists a slight variance in the carrier concentrations between the samples, due to small differences in experimental conditions between batches that influence μ. Above 650 K, the hole concentration appears to abruptly increase by several orders of magnitude for all samples. In reality, we believe this to be an artifact caused by the complex nature of the details of the valence bands that results in the failure of the single-band approximation. Additional work between our research groups to be reported elsewhere indicates that thermally excited electrons propagate from the heavy to the light hole band, producing holes in the heavy hole band. The hole mobilities in this system are similar to previously reported values for p-type PbTe, Figure 5B, generally between 100 and 250 $cm^2/(V \cdot s)$ at room temperature.[19]

Powder X-ray Diffraction (PXRD) and Analysis of Lattice Parameters of Na-Doped PbTe, PbS, and PbTe−PbS. Figure 6A shows representative powder X-ray diffraction (PXRD) patterns for PbTe−PbS thermoelectric materials. Only two phases are observed for PbTe and PbS. The PbS phase is generally observed at compositions greater than 8%. Despite the doping of 2% Na onto the Pb sites of PbTe and PbS, we do not see any evidence of a separate Na-chalcogen rich phase. The powder diffraction measurements help to explain why the 2% Na-doped PbTe−PbS 12% composition produces the highest ZT. The PbTe lattice parameters obtained from Le Bail refinements to the PXRD data are plotted in Figure 6B. The lattice parameter shrinks as small amounts of S are substituted for Te, and the total substitution can be compared to the expected trend for a complete solid solution that would follow Vegard's law (dashed line). Surprisingly, we observe a minimum in lattice parameter at PbTe−PbS 12%, indicating the maximum solubility of PbS in the PbTe matrix at this composition. The lattice parameters for all mixed compositions deviate slightly from Vegard's trend, which suggests the presence of a small amount of nanoscale phase separation of PbS that is below the resolution of the measurement. For the PbTe−PbS 16 and 30% samples, the relative increase in lattice parameter indicates a slight decrease in the solubility of PbS versus the 8% and 12% samples. We believe the differences in solubilized PbS within the PbTe matrix for PbTe−PbS 8% and 12% to have serious implications on the electronic structure of the PbTe matrix. Figure 7 is a qualitative schematic illustrating the expected depression of the light hole band as increased PbS is alloyed in PbTe, to be discussed later.

Scanning Transmission Electron Microscopy and Transmission Electron Microscopy (S/TEM) of Na-Doped PbTe−PbS. To better understand the origins of phase separation in Na-doped PbTe−PbS materials, we have conducted a detailed S/TEM study of the aforementioned PbTe, PbS, and PbTe−PbS samples. Microstructural analysis using TEM revealed two types of PbS precipitates in the samples: (a) randomly shaped with a size distribution of 1−10 nm, and (b) well-faceted nanometer scale cuboctahedral precipitates with an average edge length of 100 nm. In comparison to the n-type system, where rapid quenching from the liquid phase can generate solid solution alloys of PbTe−PbS,[28,37,38] we observed precipitation of the PbS structures even after rapid cooling for all Na-containing samples. This implies that the kinetics of phase separation are accelerated when Na is added as a dopant. Indeed, rapid kinetics are necessary to provide shape-controlled nanostructures, as has been described at length in solution chemistry.[39] For PbTe−PbS

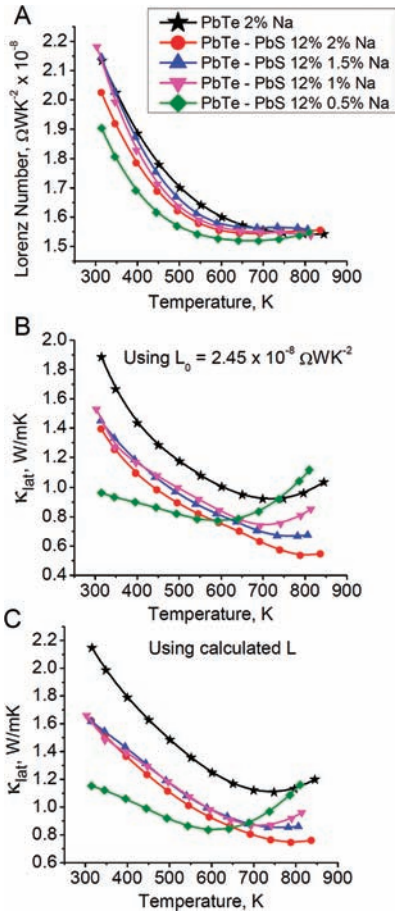

Figure 4. (A) Calculated Lorenz number, (B) lattice thermal conductivity using L_0, and (C) lattice thermal conductivity using calculated L from (A) for 2%, 1.5%, 1%, and 0.5% Na-doped PbTe−PbS 12% thermoelectric materials. Na doping also has a vital chemical effect in reducing lattice thermal conductivity in addition to enhancing power factor.

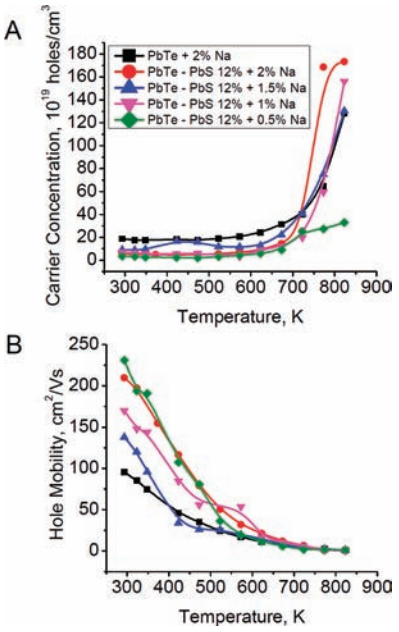

Figure 5. (A) Hole carrier concentration and (B) hole mobility of 2% PbTe and variably Na-doped PbTe−PbS 12% materials. The apparent increase in hole concentration above 650 K is an artifact resultant of the promotion of holes from the light to heavy hole band of PbTe, indicating a failure of the single-band approximation.

12%, when 1% Na is added as a dopant, we observe many of the PbS nanostructures adopting a truncated cube morphology bound by the [100] and [111] crystallographic planes. Upon addition of more Na up to 2%, we observe the PbS nanostructures to complete their growth into full nanocubes, devoid of truncation along the [111] planes.

Figure 8A and B shows low magnification images of PbTe−PbS 8% and PbTe−PbS 12% doped with 2% Na, respectively. The inset in Figure 8A shows a typical magnified TEM image with regular rectangular-shaped nanoparticles with the precipitate and matrix interfaces along the [100] or [010] directions, which is the projection of the nanocube along [001] axis as pointed by the arrowhead. The electron diffraction pattern in the inset of Figure 8B with an aperture including the PbS nanocube precipitate and PbTe matrix shows splitting of each diffracted spot, confirming the two separate phases (i.e., matrix and cubic precipitate) and their excellent endotaxial crystallographic alignment. All of the diffraction spots can be indexed with PbTe and PbS. The lattice image in the inset of Figure 8B is a typical HRTEM image of a small irregularly shaped precipitate. In Figure 8C, the low magnification image of 1% Na-doped PbTe−PbS 12% also shows truncated nanocubes in addition to the nanocubes. The inset is a projection of a truncated nanocube, which clearly shows the [100] and [111] planes. In Figure 8D and inset, the images show randomly shaped, low number density medium precipitates besides the small irregularly shaped precipitates. In comparison with undoped and n-type PbTe−PbS, which produce randomly shaped PbS particles,[28] here the precipitation dynamics have been significantly altered to allow for some degree of shape control of the minor phase. There has been much research related to shape control of PbS nanoparticles within a liquid solution;[40] here, we show that the shape of nanoparticles semicoherently embedded within a bulk matrix may be controlled as well. To the authors' best knowledge, this is the first demonstration of shape control of naturally phase-separated nanoprecipitates in bulk semiconductors.

High-Temperature Measurements of 2% Na-Doped PbTe and PbTe−PbS 12%. To verify the accuracy of our measurements, and to investigate even higher temperature transport properties, we measured the PbTe and PbTe−PbS 12% (doped with 2% Na) samples for high-temperature thermoelectric properties on a homemade system available at UM (maximum operating temperature of 850 K). To avoid outgassing, we coated the samples with a layer of boronitride, leaving only small areas uncovered to allow for placement of contacts. The high-temperature electronic transport data for the measurements are shown in Figure 9A−C. Silver paint contacts in the UM system lend to better electronic contact and a slightly enhanced measured electrical conductivity for both samples. The power factor for PbTe−PbS 12% remains well above 20 μW/cm·K^2 because of the novel temperature dependence in thermopower, eventually surpassing the power factor of the benchmark 2% Na-doped PbTe at temperatures above 700 K, Figure 9C. Additionally, the power factor remains above 20 μW/cm·K^2 for an impressive 500 °C. Using calculated values of Lorenz number, we show the introduction of nanostructures in PbTe−PbS 12% reduces the lattice thermal conductivity by 50% relative to pure

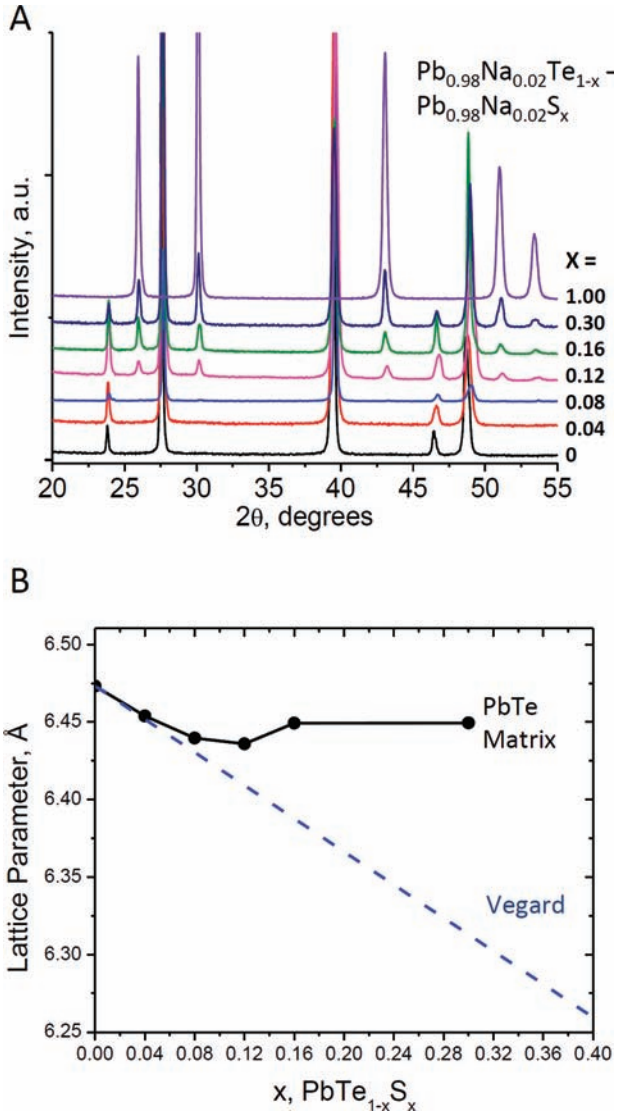

Figure 6. (A) PXRD of 2% Na-doped PbTe, PbS, and PbTe−PbS thermoelectric materials. All peaks correspond to PbTe and PbS. No impurity peaks associated with Na are observed. (B) Refined lattice parameters from PXRD data shown in (A) exhibiting variation in lattice parameter with relative PbS concentration alloyed within the PbTe matrix (black dots). The decrease in lattice parameter shows that the maximum PbS alloying occurs for the PbTe−PbS 12% composition, followed by PbTe−PbS 8%. The PbTe−PbS 4%, 16%, and 30% compositions all have similar lattice parameters and thus comparable PbS substitution within the PbTe matrix. Deviation from complete alloying, as shown by the Vegard trend (dotted line), is a result from nanoscale phase separation of PbS. Error bars are smaller than symbols for all points. The increased dissolution of PbS in the PbTe matrix to form $PbTe_{1-x}S_x$ has a significant impact on the electronic valence band structure of the material.

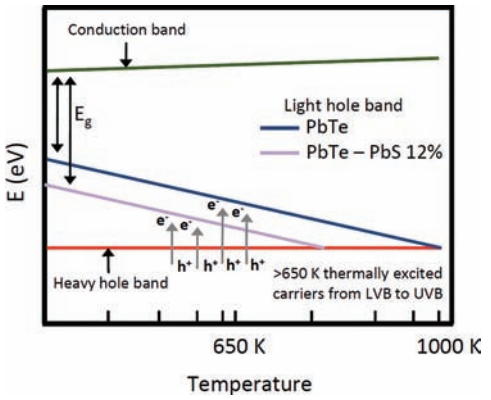

Figure 7. Schematic showing shift of valence band extrema of PbTe and PbTe−PbS 12% with temperature. As increased PbS is dissolved in the PbTe matrix, the light hole valence band of PbTe is lowered in energy (increase in band gap E_g), decreasing the difference in energy between the light and heavy hole bands. At elevated temperatures, thermally excited carriers traverse from the heavy to light hole bands, increasing the population of heavy holes and enhancing thermopower at elevated temperatures.

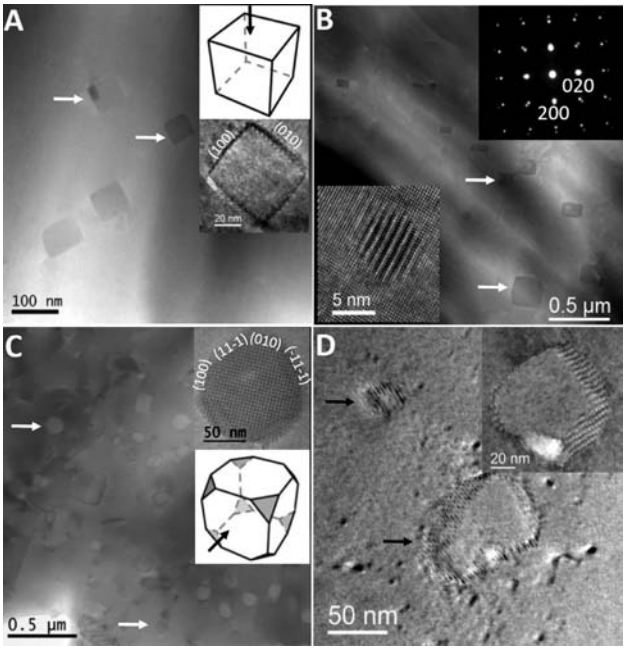

Figure 8. S/TEM images that show shape control of PbS nanocrystals by tuning the Na concentration. For samples containing (A) PbTe−PbS 8% + Na 2% and (B) PbTe−PbS 12% + Na 2%, a high density of fully cubic PbS nanocrystals are observed along the [100] crystallographic planes. The cubes are terminated along the [010] and [100] planes. (C) As the Na concentration is reduced to PbTe−PbS 12% + Na 1%, truncated cubes are formed with additional facets along the [111] crystallographic planes. (D) As the Na doping is further reduced to PbTe−PbS 12% + Na 0.5%, randomly shaped PbS precipitates are observed.

PbTe at 800 K, Figure 10A. Again, we must stress that we are underestimating the Lorenz number because we neglect the contribution of the heavy hole band, and therefore the actual lattice thermal conductivity should be even lower. Despite this, we can explicitly show an advantageous reduction in lattice thermal conductivity. Because of the dual enhancement in power factor and reduction in lattice thermal conductivity for 2% Na-doped PbTe−PbS 12%, we report a maximum ZT of 1.8 at 800 K, Figure 10B. In light of the significant errors that may arise from thermoelectric properties measurements (from 3% to 6%), we have added 10% error bars in Figure 10B to illustrate the expected instrumental and experimental deviation in the thermoelectric figure of merit.

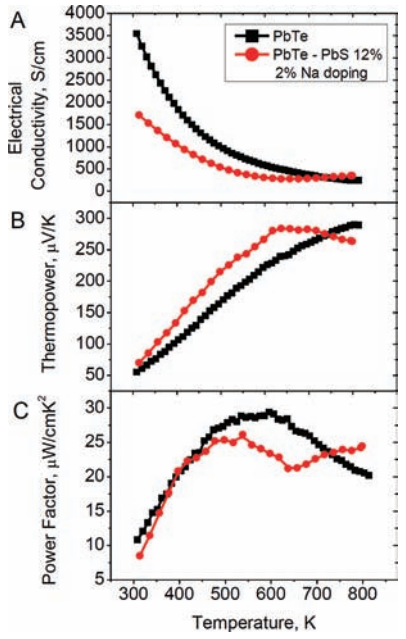

Figure 9. High-temperature (A) electrical conductivity, (B) thermopower, and (C) power factor of 2% Na-doped PbTe and PbTe−PbS 12%.

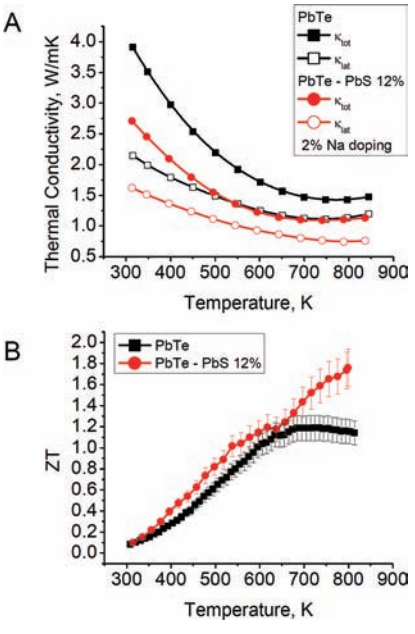

Figure 10. High-temperature (A) total and lattice thermal conductivity and (B) ZT of 2% Na-doped PbTe and PbTe−PbS 12%. In (A), the lattice thermal conductivity was obtained as described for Figures 2 and 4. At 800 K, the lattice thermal conductivity of the PbTe−PbS 12% sample is reduced by at least 50%. Because of the enhancement in power factor and extremely low lattice thermal conductivity, a ZT of 1.8 at 800 K is achieved for the 2% Na-doped PbTe−PbS 12% sample.

DISCUSSION

The above results clearly suggest there are two effects through the addition of PbS and Na in PbTe: modification of the electronic structure and reductions in lattice thermal conductivity, jointly contributing to a superior figure of merit. In particular, the novelty of the electronic transport is of great importance. Such behavior cannot be attributed to bipolar diffusion, as a similar rise in *n* is not observed for analogous n-type PbTe−PbS samples, nor for PbS−PbTe materials.[27,28,33] For typical bipolar diffusion, thermally induced cross-gap excitations of minority carriers (i.e., electrons) will increase electrical conductivity, while the increased overall carrier concentration will reduce thermopower and significantly increase the electronic contribution to thermal conductivity. Indeed, this is what we clearly observe in the bell-shaped curves in thermopower for the 0.5% Na-doped PbTe−PbS 12% at 675 K, Figure 3B, as well as 2% Na-doped PbTe at 875 K, Figure 10B. However, bipolar diffusion cannot explain the plateau-like thermopower transport in the 1−2% Na-doped PbTe−PbS 12% samples, Figure 3B. We suggest the novel transport properties to be the result of promotion of holes from the light to heavy hole valence bands in PbTe. The incorporation of PbS is necessary to observe these effects, suggesting the positions of the light and heavy hole bands are altered through the alloying of PbTe and PbS. Additionally, there must be a significant density of holes present. We observe that hole densities >3 × 10^{19} holes/cm^3 are required for sufficient promotion of holes in PbTe−PbS 12% from the light to heavy hole bands at high temperature and produce the desired enhancements in power factor.

That we see increased PbS alloy substitution into the PbTe matrix for the PbTe−PbS 8% and 12% compositions is a vital finding toward understanding the superior thermoelectric performance of these materials. To qualitatively describe our argument, we have provided a schematic in Figure 7. Despite similarities in crystal structure, the difference in the chemical structure in PbTe and PbS produces room temperature band gaps of ∼0.30 and ∼0.41 eV, respectively. As more sulfur is substituted for Te within PbTe, the band gap increases as the top of the light hole valence band of PbTe is decreased in energy without significantly affecting the heavy hole band. This has been observed recently on the PbS-rich side of the PbTe−PbS system.[33] As a result of this depression, at higher temperatures, significantly more thermally excited holes may be generated in the heavy hole band of PbTe, producing the novel electronic properties we report. We observe these properties in all PbS-containing materials; however, the highest thermopower observed is from the PbTe−PbS 12% composition, whose band gap should be largest as a result of increased alloying between the PbTe and PbS phases. Further studies are currently underway to understand the role of the heavy hole band and its temperature dependence.

In the $PbTe_{1-x}S_x$ system, phase separation occurs by nucleation and growth, spinodal decomposition, or some mixture thereof. The differences in the thermodynamic process by which the materials phase separate may explain the relative differences in PbS alloying within the PbTe matrix. From the phase diagram, at temperatures around 773 K, spinodal decomposition in $PbS_{1-x}Te_x$ occurs toward the middle of the phase space, while nucleation and growth occur toward the outer phase space.[41,42] Therefore, the PbTe−PbS 4%, 8%, and 12% compositions should phase separate according to a nucleation and growth phase transformation, while the PbTe−PbS 16% is a mix of both transformations, and the 30% composition phase separates only by spinodal decomposition.[27] According to the Lever rule, the samples will reach thermal equilibrium at the composition of the outer binodal line as shown in the phase diagram; because of this, we might expect the phases to have similar composition given

identical heat treatment. However, here incorporation of Na is vital in altering the phase stability of PbTe−PbS. Additionally, distinction between the thermodynamically unstable spinodal decomposition and the metastable nucleation and growth transformations may further explain the relative differences in phase composition between the samples. Differences in the thermodynamic instability in the PbTe−PbS 16% and 30% compositions may initiate phase separation more readily than for the PbTe−PbS 4%, 8%, and 12% compositions, producing more significantly phase separated samples.

It has been established that for lead chalcogenides, and more specifically PbS nanostructures, shape-control may be achieved by altering the relative ratio in the growth rate γ between the [100], [111], and [110] crystallographic planes. Generally, the surface energies within PbS nanostructures follow $\gamma_{[111]} < \gamma_{[100]} < \gamma_{[110]}$.[43] To create cubic morphologies, the ratio in the growth rate of the [100] and [111] directions must be approximately 0.58; to create truncated cube morphologies, the ratio is between 0.87 and 1.73. From our findings, we can see experimentally that there exist clear differences in growth between the [100] and [111] planes dependent on Na doping. Ongoing work in our lab suggests that the formation enthalpies of nominal PbTe−PbS solid solutions are reduced along the [111] direction; it would appear that the substitution of even 0.5−2% Na significantly alters the surface reactivity of the precipitated PbS nanocrystals, producing shape-controlled nanostructures. In a future publication, we will investigate the role of the PbTe/PbS interface by STEM EDS and Local-Electrode Atom-Probe (LEAP) tomography. Through this, we may better understand the potential of Na segregation at different interfacial planes as a means to create the anisotropic PbS nanostructures.

SUMMARY

We have demonstrated a successful thermoelectric material system exhibiting enhancements as a result of two concurrent effects: nanostructuring to reduce lattice thermal conductivity, and enhancement of power factor through band structure modification. We have also shown for the first time that the Na-doped PbTe−PbS system is not only nanostructured but exhibits shape-controlled nanocrystals of PbS embedded throughout the matrix, which we submit is mediated by the presence of Na ions. This is in contrast to the n-type PbTe−PbS system, reported previously, which exhibits a different kind of nanostructuring with a random size and shape of precipitates. While these shape-controlled nanoparticles are vital at reducing lattice thermal conductivity, extensions of this top-down nanostructuring approach may also have important implications controlling key features in catalysis, electronics, optics, plasmonic, and other potential applications. There are recent reports of high ZT in PbTe-based materials prepared by powder processing and subsequent hot pressing.[21,22] For example, a sample of 2% Na-doped PbTe that has been milled and hot pressed has been reported to have a ZT of 1.5 at 750 K, in contrast to our finding of ZT 1.1 at 750 K for a cast ingot of the same composition. Barring any experimental errors associated with the measurements, it would appear that the powder processing and mechanical pressing of PbTe materials may plausibly reduce the thermal conductivity and surprisingly enhance the electrical conductivity. This may prove a useful approach toward enhancing the thermoelectric figure of merit in PbTe-based materials, potentially raising the ZT of the PbTe−PbS 12% samples in this Article to ZT values approaching 2.

ASSOCIATED CONTENT

Supporting Information. Description of high-temperature thermoelectric measurements, Figures S1 and S2, diffusivity measurements and description of high-temperature analysis of diffusivity data, Figures S3 and S4, specific heat values used, Figure S5, measured sample densities, Table S1, measured Hall coefficient values, Figure S6, and lattice parameters determined by Le Bail refinement, Table S2. This material is available free of charge via the Internet at http://pubs.acs.org.

AUTHOR INFORMATION

Corresponding Author
m-kanatzidis@northwestern.edu

ACKNOWLEDGMENT

The work is supported as part of the Revolutionary Materials for Solid State Energy Conversion, an Energy frontier Research Center funded by the U. S. Department of Energy, Office of Basic Energy Sciences under Award Number DE-SC0001054. Many thanks are due to Drs. John Androulakis and Simon Johnsen for valuable discussions. The SEM and TEM work was performed in the EPIC facility of the NUANCE Center at Northwestern University. The NUANCE Center is supported by NSF-NSEC, NSF-MRSEC, Keck Foundation, the State of Illinois, and Northwestern University.

REFERENCES

(1) Kanatzidis, M. G. *Chem. Mater.* **2009**, *22*, 648.
(2) Li, H.; Tang, X.; Zhang, Q.; Uher, C. *Appl. Phys. Lett.* **2009**, *94*, 102114.
(3) Lan, Y.; Minnich, A. J.; Chen, G.; Ren, Z. *Adv. Funct. Mater.* **2010**, *20*, 357.
(4) Boukai, A. I.; Bunimovich, Y.; Tahir-Kheli, J.; Yu, J.-K.; Goddard Iii, W. A.; Heath, J. R. *Nature* **2008**, *451*, 168.
(5) Venkatasubramanian, R.; Silvola, E.; Colpitts, T.; O'Quinn, B. *Nature* **2001**, *413*, 597.
(6) Dresselhaus, M. S.; Chen, G.; Tang, M. Y.; Yang, R. G.; Lee, H.; Wang, D. Z.; Ren, Z. F.; Fleurial, J.-P.; Gogna, P. *Adv. Mater.* **2007**, *19*, 1043.
(7) Hochbaum, A. I.; Chen, R.; Delgado, R. D.; Liang, W.; Garnett, E. C.; Najarian, M.; Majumdar, A.; Yang, P. *Nature* **2008**, *451*, 163.
(8) Rao, A. M.; Ji, X.; Tritt, T. M. *MRS Bull.* **2006**, *31*, 218.
(9) Sootsman, J. R.; Chung, D. Y.; Kanatzidis, M. G. *Angew. Chem., Int. Ed.* **2009**, *48*, 8616.
(10) Sootsman, J. R.; Pcionek, R. J.; Kong, H.; Uher, C.; Kanatzidis, M. G. *Chem. Mater.* **2006**, *18*, 4993.
(11) Hsu, K. F.; Loo, S.; Guo, F.; Chen, W.; Dyck, J. S.; Uher, C.; Hogan, T.; Polychroniadis, E. K.; Kanatzidis, M. C. *Science* **2004**, *303*, 818.
(12) Alboni, P. N.; Ji, X.; He, J.; Gothard, N.; Tritt, T. M. *J. Appl. Phys.* **2008**, *103*, 113707.
(13) Snyder, G. J.; Toberer, E. S. *Nat. Mater.* **2008**, *7*, 105.
(14) Nolas, G. S.; Poon, J.; Kanatzidis, M. *MRS Bull.* **2006**, *31*, 199.
(15) Chiritescu, C.; Cahill, D. G.; Heideman, C.; Lin, Q.; Mortensen, C.; Nguyen, N. T.; Johnson, D.; Rostek, R.; Böttner, H. *J. Appl. Phys.* **2008**, *104*, 033533.
(16) Bux, S. K.; Blair, R. G.; Gogna, P. K.; Lee, H.; Chen, G.; Dresselhaus, M. S.; Kaner, R. B.; Fleurial, J.-P. *Adv. Funct. Mater.* **2009**, *19*, 2445.

(17) Heremans, J. P.; Jovovic, V.; Toberer, E. S.; Saramat, A.; Kurosaki, K.; Charoenphakdee, A.; Yamanaka, S.; Snyder, G. J. *Science* **2008**, *321*, 554.
(18) (a) Jaworski, C. M.; Kulbachinskii, V.; Heremans, J. P. *Phys. Rev. B* **2009**, *80*, 233201. (b) He, J. Q.; Sootsman, J. R.; Girard, S. N.; Zheng, J. C.; Wen, J. G.; Zhu, Y. M.; Kanatzidis, M. G.; Dravid, V. P. *J. Am. Chem. Soc.* **2010**, *132*, 8669–8675. (c) He, J. Q.; Gueguen, A.; Sootsman, J. R.; Zheng, J. C.; Wu, L. J.; Zhu, Y. M.; Kanatzidis, M. G.; Dravid, V. P. *J. Am. Chem. Soc.* **2009**, *131*, 17828–17835.
(19) (a) Biswas, K.; He, J.; Zhang, Q.; Wang, G.; Uher, C.; Dravid, V. P.; Kanatzidis, M. G. *Nat. Chem.* **2011**, *3*, 160. (b) Ahn, K.; Han, M. K.; He, J. Q.; Androulakis, J.; Ballikaya, S.; Uher, C.; Dravid, V. P.; Kanatzidis, M. G. *J. Am. Chem. Soc.* **2010**, *132*, 5227–5235. (c) Gueguen, A.; Poudeu, P. F. P.; Li, C. P.; Moses, S.; Uher, C.; He, J. Q.; Dravid, V.; Paraskevopoulos, K. A.; Kanatzidis, M. G. *Chem. Mater.* **2009**, *21*, 1683–1694.
(20) Androulakis, J.; Todorov, I.; Chung, D.-Y.; Ballikaya, S.; Wang, G.; Uher, C.; Kanatzidis, M. *Phys. Rev. B* **2010**, *82*, 115209.
(21) Pei, Y.; LaLonde, A.; Iwanaga, S.; Snyder, G. J. *Energy Environ. Sci.* **2011**, *4*, 2085−2089.
(22) Pei, Y.; Shi, X.; LaLonde, A.; Wang, H.; Chen, L.; Snyder, G. J. *Nature* **2011**, *473*, 66.
(23) Allgaier, R. S.; Houston, B. B. *J. Appl. Phys.* **1966**, *37*, 302.
(24) Allgaier, R. S. *J. Appl. Phys.* **1961**, *32*, 2185.
(25) Kolomoets, N. V.; Vinogradova, M. N.; Sysoeva, L. M. *Sov. Phys. Semicond.* **1968**, *1*, 1020.
(26) Kudman, I. *J. Mater. Sci.* **1972**, *7*, 1027.
(27) Androulakis, J.; Lin, C.-H.; Kong, H.-J.; Uher, C.; Wu, C.-I.; Hogan, T.; Cook, B. A.; Caillat, T.; Paraskevopoulos, K. M.; Kanatzidis, M. G. *J. Am. Chem. Soc.* **2007**, *129*, 9780.
(28) Girard, S. N.; He, J.; Li, C.; Moses, S.; Wang, G.; Uher, C.; Dravid, V. P.; Kanatzidis, M. G. *Nano Lett.* **2010**, *10*, 2825.
(29) Mayer, J.; Giannuzzi, L. A.; Kamino, T.; Michael, J. *MRS Bull.* **2005**, *32*, 400.
(30) Crocker, A. J. *J. Phys. Chem. Solids* **1967**, *28*, 1903.
(31) Nemov, S. A.; Ravich, Y. I. *Phys.-Usp.* **1998**, *41*, 735.
(32) May, A. F.; Toberer, E. S.; Snyder, G. J. *J. Appl. Phys.* **2009**, *106*, 013706.
(33) Johnsen, S.; He, J.; Androulakis, J.; Dravid, V. P.; Todorov, I.; Chung, D. Y.; Kanatzidis, M. G. *J. Am. Chem. Soc.* **2011**, *133*, 3460.
(34) Tamarchenko, V. I.; Ravich, Y. I.; Morgovskii, L. Y.; Dubrovskaya, I. N. *Sov. Phys. Solid State* **1970**, *11*, 2599.
(35) Ravich, Y. I.; Smirnov, I. A.; Tikhonov, V. V. *Sov. Phys. Semicond.* **1967**, *1*, 163.
(36) May, A. F.; Toberer, E. S.; Saramat, A.; Snyder, G. J. *Phys. Rev. B* **2009**, *80*, 125205.
(37) He, J.; Girard, S. N.; Kanatzidis, M. G.; Dravid, V. P. *Adv. Funct. Mater.* **2010**, *20*, 764.
(38) Girard, S. N.; He, J.; Dravid, V. P.; Kanatzidis, M. G. *Mater. Res. Soc. Symp. Proc.* **2009**, *1166*, 59.
(39) Tao, A. R.; Habas, S.; Yang, P. *Small* **2008**, *4*, 310.
(40) Zhou, G.; Lü, M.; Xiu, Z.; Wang, S.; Zhang, H.; Zhou, Y.; Wang, S. *J. Phys. Chem. B* **2006**, *110*, 6543.
(41) Darrow, M. S.; White, W. B.; Roy, R. *Mater. Sci. Eng.* **1969**, *3*, 289.
(42) Volykhov, A.; Yashina, L.; Shtanov, V. *Inorg. Mater.* **2006**, *42*, 596.
(43) Wang, Z. L. *J. Phys. Chem. B* **2000**, *104*, 1153.